Journal of Power Sources 195 (2010) 6611–6618

Contents lists available at ScienceDirect

Journal of Power Sources

journal homepage: www.elsevier.com/locate/jpowsour

A durability model for solid oxide fuel cell electrodes in thermal cycle processes

Yanxiang Zhang, Changrong Xia*

CAS Key Laboratory of Materials for Energy Conversion, Department of Materials Science and Engineering, University of Science and Technology of China, 96 Jinzhai RD, Hefei, 230026 Anhui, China

ARTICLE INFO

Article history:
Received 3 March 2010
Received in revised form 15 April 2010
Accepted 15 April 2010
Available online 22 April 2010

Keywords:
Solid oxide fuel cell
Nanostructured electrode
Durability model
Thermal cycle

ABSTRACT

Despite the intense interest in solid oxide fuel cells, many details of their durability remain a mystery. Here, we present the insight see on electrode degradation in thermal cycle processes. Our model interprets the degradation to the stresses induced by thermal expansion mismatch of the electrocatalyst and electrolyte in a composite electrode that undergoes a temperature change. Such stresses might break the particle–particle interfaces (grain boundaries), thus reduce oxygen-ionic conductivity, electronic conductivity, and three-phase boundaries within the electrode, and consequently, degrade its performance. The model formulates the degradation rate as a function of cycle number, thermal expansion coefficient, composition, and particle size, providing a remarkable ability to balance thermal expansion restriction and catalytic activity of electrode materials, to optimize the electrode structure and composition, and to predict thermal-cycle durability. The model explicitly demonstrates that, in addition to their excellent electrochemical activity, nanostructured electrodes exhibit exceptional durability in thermal cycle processes.

1. Introduction

Solid oxide fuel cells (SOFCs) are a forward looking technology for highly efficient, environmental friendly power generation [1–5]. A SOFC is a multilayer structure consisting of at least three functional components: anode, electrolyte and cathode. All components have to show a well matched thermal expansion behavior so that the multilayer structure could function well in thermal cycle processes including start-up and shut-down [6]. Unfortunately, thermal expansion coefficients (TECs) of electrocatalysts such as lanthanum strontium manganite, lanthanum strontium cobaltite, and nickel are usually different from that of electrolytes. Therefore, there is always electrode degradation in the thermal cycle processes. However, details of the degradation process are still not available for electrodes with different TECs and various structures.

The present work provides the insight into electrode durability in thermal cycle processes. A model is developed to quantitatively predict the electrode performance in terms of interfacial polarization resistance with respect to thermal cycle number, electrocatalyst TEC, temperature change, and electrode characteristics including composition, microstructure, and particle size. The model is interpreted here with the cathode but can also be used to evaluate the anode durability. In addition, the model is applicable to other solid-state electrochemical devices that undergo temperature changes.

2. Model description

In the cathode, oxygen is electrochemically reduced to oxygen ion via the overall half-cell reaction,

$$2e^- + \frac{1}{2}O_2 = O^{2-}$$

Therefore, the reaction occurs at so-called three-phase boundary (TPB) where oxygen-ion, electron, and oxygen are available [7]. In a porous composite cathode consisting of an electrocatalyst and an electrolyte, TPB is created when an oxygen-ionic conducting (the electrolyte, i phase) particle is bonded to an electronic conducting (the electrocatalyst, j phase) particle, forming an i–j interface between the two phases (Fig. 1). The TPB is active if only the electrocatalyst particle is connected to the percolated electronic phase through forming a j–j interface (grain boundary) with its adjacent electrocatalyst particle that belongs to the electronic conducting network. Similarly, to activate the TPB, an i–i interface (grain boundary) must be formed between the electrolyte particle and its neighboring electrolyte particle that belongs to the ionic conducting network of the composite cathode. The reaction will not happen if any of the three interfaces breaks: the i–j interface breaking destroys the TPB, the i–i breaking blocks the oxygen ion transportation route, and the j–j breaking terminates the electron supply. These interfaces are usually formed with high temperature related processes and often strong enough to withstand the harsh SOFC operating conditions. When thermal expansion coefficient (TEC) of the electrolyte (α_i) and the electrocatalyst (α_j) are different, the interface could be broken by a misfit strain ($\Delta\varepsilon$) resulted from a temperature change, ΔT (positive for heating and negative

* Corresponding author. Tel.: +86 551 3607475; fax: +86 551 3601592.
E-mail address: xiacr@ustc.edu.cn (C. Xia).

0378-7753/$ – see front matter © 2010 Elsevier B.V. All rights reserved.
doi:10.1016/j.jpowsour.2010.04.051

Nomenclature

D	degradation rate (%)
E	Young's modulus for dense materials (GPa)
$\tilde{E}$	effective Young's modulus (GPa)
I	current density (mA cm^{-2})
L	electrode thickness (μm)
m	Weibull parameter
N	cycle number
P	survival probability
p	percolation probability
R	resistance (Ω cm^{-2})
r	particle radius (μm)
ΔT	temperature change (°C)
V	voltage (V)
W	power density (mW cm^{-2})
Z	coordination number

Greek letters

α	thermal expansion coefficient (K^{-1})
$\Delta\varepsilon$	misfit strain
ϕ	volume fraction
ν	Poisson ratio
ρ	resistivity (Ω cm)
Σ	Weibull parameter (N cm$^{-11/15}$)
σ	stress (GPa)

Superscripts

eff	effective value
E	electrolyte
C	cathode
A	anode

Subscripts

ave	average value
g	pore
i	ionic conducting phase
j	electronic conducting phase
s	survival

for cooling),

$$\Delta\varepsilon = (\alpha_j - \alpha_i)\Delta T \tag{1}$$

At a stress balance state, imposition of this misfit strain results in a couple of equal and opposite stresses, σ_i in the electrolyte phase and σ_j in the electrocatalyst phase, holding $\sigma_i = -\sigma_j = \sigma$. So,

$$\Delta\varepsilon = \sigma\left(\frac{1}{\tilde{E}_i} + \frac{1}{\tilde{E}_j}\right) \tag{2}$$

where $\tilde{E}_i$ and $\tilde{E}_j$ are the effective modulus of electrolyte and electrocatalyst phases, respectively. According to the power law expression [8], they can be simplified as,

$$\tilde{E}_i = \frac{E_i}{1-2\nu}\phi_i(1-\phi_g) \tag{3-a}$$

$$\tilde{E}_j = \frac{E_j}{1-2\nu}\phi_j(1-\phi_g) \tag{3-b}$$

where ϕ_g represents the cathode porosity, ϕ_i and ϕ_j denote the volume fraction of ionic and electronic phases relative to the total solid materials, with the porosity ϕ_g specified independently. E_i and E_j are the Young's modulis corresponding to fully dense materials. ν is the Poisson ratio. The TEC of the whole cathode can be estimated as [9],

$$\alpha_{ave} = \frac{\alpha_i\tilde{E}_i + \alpha_j\tilde{E}_j}{\tilde{E}_i + \tilde{E}_j} \tag{4}$$

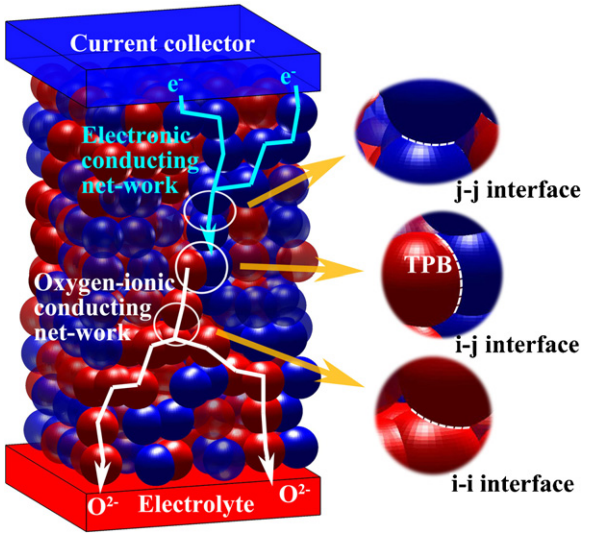

Fig. 1. Illustration for a three-phase boundary (TPB), particle–particle interfaces, and conducting networks, in a composite cathode consisting of electrocatalyst (blue), electrolyte (red), and pores (transparent). (For interpretation of the references to color in this figure legend, the reader is referred to the web version of this article.)

The interfaces between the two phases are assumed to belong to either the ionic phase or the electronic phase. That is, the stress in the interfaces of the two phases, σ_{i-j}, is equal to σ in absolute value, and its direction is set to be the same as ionic phase. It is the stresses that break the interface, resulting in the reduction of TPB, and consequently, degradation in electrochemical performance with respect to temperature change processes such as thermal cycle. Fortunately, the interface may survive sometimes. The survival probability, $P_{s,i-j}$, under positive stress σ can be estimated with Eq. (5), which is derived from the Weibull weakest-link theory [10,11],

$$P_{s,i-j}(\sigma) = \exp\left(-r_{i-j}^2\left(\frac{\sigma}{\Sigma_{i-j}}\right)^{m_{i-j}}\right) \tag{5}$$

where Σ_{i-j} and m_{i-j} are Weibull paremeters corresponding to the interface between i and j phase, r_{i-j} is the smaller particle radius of i and j phase, i.e., the size of the nanosized particles in case of nanostructured electrodes. Eq. (5) suggests high survival probability is associated with smaller size. For simplification, the effect of electrolyte layer on electrode-structure failure is attributed to Σ_{i-j}, and the validity is shown in Fig. 2a. After N thermal cycles, the number of effective contacts (survival interfaces) between an i phase particle and j phase particles, $Z_{i-j,N}$, is given by,

$$Z_{i-j,N} = Z_{i-j}P_{s,i-j}^N \tag{6}$$

Z_{i-j} denotes the initial interface number (coordination number), which is a function of electrode composition and particle sizes. Eq. (6) reveals an exponentially decreasing rule of survival coordination numbers as a function of thermal cycle number. The interfacial polarization resistance, R_p, strongly depends upon the interface number according to the particle-layer model [12],

$$R_p = \sqrt{\frac{\rho_{TPB}^{eff}\rho_i^{eff}}{ln_i p_i p_j Z_{i-j,N}}}\ \coth\left(L\sqrt{\frac{\rho_i^{eff} ln_i p_i p_j Z_{i-j,N}}{\rho_{TPB}^{eff}}}\right) \tag{7}$$

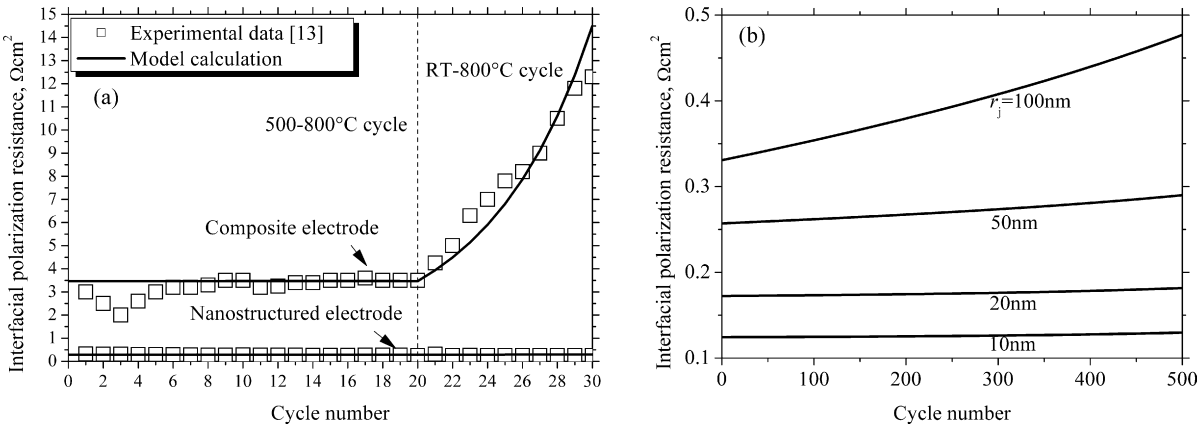

Fig. 2. Interfacial polarization resistances (600 °C) for LSC-based cathodes on SDC electrolytes. (a) Comparison between model prediction and experimental result [13] for LSC–SDC composite cathode and nanostructured cathode in thermal cycle processes ($\phi_i = \phi_j = 0.5$, $\phi_g = 0.41$, $r_i = 1$ μm, and $r_j = 1$ μm for composite cathode; $r_i = 1$ μm and $r_j = 50$ nm for nanostructured cathode). (b) Effects of nanoparticle size for LSC–SDC nanostructured cathode under thermal cycle treatment ($\phi_i = \phi_j = 0.5$, $\phi_g = 0.41$, $r_i = 0.5$ μm, and RT–800 °C cycle).

where L is the thickness of cathode. ρ_{TPB}^{eff} and ρ_i^{eff} indicate the effective resistivity of TPB and ionic phase, respectively. l is the neck perimeter between an ionic particle and an electronic particle, n_i is the number of ionic particles per unit volume. p_i and p_j denote the percolation probabilities of the ionic and electronic particles. Similarly, the stresses could break the interface between two electronic particles and the interface of two ionic particles, and thus reduce the coordination numbers for the same-phase particle. However, for a composite cathode, the effects of $Z_{i-i,N}$ and $Z_{j-j,N}$ on interfacial polerazation resistance are more complex, due to their effects on percolation probabilities,

$$p_i = \left[1 - \left(\frac{4.236 - Z_{i-i,N}}{2.472}\right)^{2.5}\right]^{0.4} \quad (8\text{-a})$$

$$p_j = \left[1 - \left(\frac{4.236 - Z_{j-j,N}}{2.472}\right)^{2.5}\right]^{0.4} \quad (8\text{-b})$$

While for a nanostructured cathode with presintered backbone [13], the percolation probabilities are both equal to 1, independent from the survival coordination numbers (see Ref. [12] for further details of the particle-layer model).

3. Results and discussion

Interfacial polarization resistances at 600 °C are calculated. The TECs and Young's moduli are assumed to be constants in the range of RT–1000 °C. Although Weibull distribution is widely accepted to characterize the structure failure of brittle materials (e.g., ceramics and low-carbon steels) [14], Weibull parameters are still difficult to find in the literature, especially for SOFC materials, due to the difficulty in manufacturing and/or testing [15]. Thus, the Weibull parameters are estimated on the basis of literature data [13], and the validity is conducted. All the electrochemical and the mechanical parameters are derived from Refs. [6,12,13,15–24,33,34] and summarized in Table 1.

3.1. Model validation

The model prediction is in excellent agreement with our previous experimental results [13]. Fig. 2a shows the performance comparison between model and our experiment for the nanostructured and composite $La_{0.6}Sr_{0.4}CoO_3$ (LSC)–$Sm_{0.2}Ce_{0.8}O_{1.9}$ (SDC) cathodes that undergo two stages of thermal cycle processes, i.e., 20 500–800 °C cycles followed by 10 RT (room temperature)–800 °C cycles. For the composite cathode, the resistance increases slightly at the first stage of thermal cycle, while it increases from 3.5 to 14.5 Ω cm² according to the model prediction, compared with the experimental data from 3.5 to 12.5 Ω cm², at the second stage. For the nanostructured electrode, the resistance remains almost constant during the two stages of thermal cycle. The nanostructured cathode can be modeled with quantitative agreement with experiment. The model is further validated with experimental data reported for a Ni-YSZ (yttria stabilized zirconia) anode and a microtubular single cell, which is discussed in Sections 3.7 and 3.8.

Table 1
Electrochemical and mechanical parameters for model calculation.

Parameter	Value	Description and reference
ρ_{TPB}^{eff}	4.5×10^5 Ω cm for LSC–SDC 5.6×10^5 Ω cm for LSCF–SDC 7.4×10^5 Ω cm for LSF–SDC 1.1×10^6 Ω cm for LSM–SDC[a]	[12,22]
α_i	11.0×10^{-6} K^{-1} for SDC 10.8×10^{-6} K^{-1} for YSZ	[13] [6]
α_j	23.0×10^{-6} K^{-1} for LSC 14.8×10^{-6} K^{-1} for LSCF 12.3×10^{-6} K^{-1} for LSF 11.7×10^{-6} K^{-1} for LSM 16.2×10^{-6} K^{-1} for Ni	[13,15,16]
E_i	100 GPa for SDC 183 GPa for YSZ	[18] [6]
E_j	60 GPa for LSC 160 GPa for LSCF 130 GPa for LSF 29.7 GPa for LSM 180 GPa for Ni	[16,17,19,20,24]
ν m_{i-i}, m_{j-j}, m_{i-j} Σ_{i-j} Σ_{i-i}, Σ_{j-j}	0.3 7.5 1.11×10^6 N cm$^{-11/15}$ 1.45×10^6 N cm$^{-11/15}$	Assumed values on the basis of literature data [13,16,17,21]
R_0^A	0.17 Ω cm² for Ni-YSZ anode	[33]
V_{OCV} I R_0^E R_0^C R_0^A	0.938 V 400 mA cm^{-2} 0.07 Ω cm² 0.24 Ω cm² 0.22 Ω cm²	Parameters for Ni-YSZ/YSZ/LSM–YSZ single cell in Ref. [34]

[a] Experimentally determined according to the method in Ref. [23].

3.2. High durability of nanostructured electrodes, the size effect

The model reveals that nanostructured cathodes have superior durability and electrochemical activity to composite cathodes. For SOFC electrodes, it has been extensively demonstrated that reducing the particle size can increase the electrochemical activity since small particles create large TPB and have high surface area for the catalytic reaction [12,25]. Cathodes with nanosized particles are therefore very attractive and have been developed via various fabrication routes [13,26–29]. Our model reveals that small size results in not only high activity but also excellent durability in the thermal cycle processes. The durability is qualitatively discussed here with a degradation rate, D_N, which is defined as $D_N = (R_N - R_0/R_0) \times 100\%$, where R_0 is the interfacial polarization resistance for the fresh electrode, R_N the resistance for the electrode undergoing N thermal cycles. Fig. 2b shows the resistances as a function of thermal cycle number for the nanostructured electrodes with different electrocatalyst size. Remarkable nanosized effect is well predicted that, with the decrease of impregnated particle size from 100 to 10 nm, both the durability and activity increase substantially. For example, after 500 cycles, the resistance increases from 0.33 to 0.48 $\Omega\,cm^2$ and the degradation rate is 45% when the size is 100 nm, whereas only slight resistance increase from 0.12 to 0.13 $\Omega\,cm^2$ and much low degradation rate of 8.3% are predicted for 10 nm particles. Therefore, for the nanostructured cathode, two benefits, i.e. enhanced electrochemical activity and pronounced durability in thermal cycle processes, are predicted while reducing the catalyst size if the nanoparticles are not sintered under SOFC operating conditions.

3.3. High durability of nanostructured electrodes, the structural effect

The model further reveals that the excellent durability is due to the small size of nanoparticles rather than the unique structure of nanostructured electrodes. As mentioned above, compared with the composite cathode, the nanostructured cathode has superior durability in thermal cycle processes. In the literature, the excellent stability is often attributed to its unique structures consisting of porous electrolyte backbones and impregnated electrocatalyst particles [13,27–29]. The backbones, which are usually sintered with the electrolyte layer at relatively high temperatures, are considered to dominate the electrode TEC and consequently, to relax the TEC match restrictions on the electrocatalysts. Our model demonstrates that the high durability is not only due to the TEC-determining backbones but also, and more importantly, due to the nanosized electrocatalysts deposited by the impregnation process (Figs. 2b and 3). In other words, it is the nanosized particles that stabilize the cathode in the thermal cycle processes. If the size of impregnated LSC particles increases to micrometer scale, say 1.0 μm, the resistance increases by 139% in 10 RT–800 °C cycles. The increase is as significant as that of the composite electrode. It should be noted that even with the same particle size and composition, a composite cathode shows a higher degradation rate than the cathode with the unique structures consisting of presintered backbones (Fig. 4). In these structures, the backbones create the oxygen-ion conducting network. All the electrolyte particles belong to the network and the inside particles are surrounded by the same-phase particles. Therefore, the effect of i–i interface breaking on the continuity of the oxygen-ion conduction network is not as severe as that for composite cathodes in which the networks are formed by percolated electrolyte particles in randomly packing systems. Consequently, performance degradation derived from the i–i interface breaking is lower for the cathode with the unique structure than that for the composite cathode. And for the nanostructured cathode, not every i–i interface breaking blocks the oxygen-ion conduction route but each i–j interface breaking reduces TPB. Thus, the durability is dominated by the survival probability of the i–j interface, which is determined by the particle size of the fine phase, the impregnated nanoparticles. And smaller particle results in higher durability (Fig. 5). So, our model demonstrates that the thermal-cycle stability originates mainly from the nanoparticles rather than from the strong backbones.

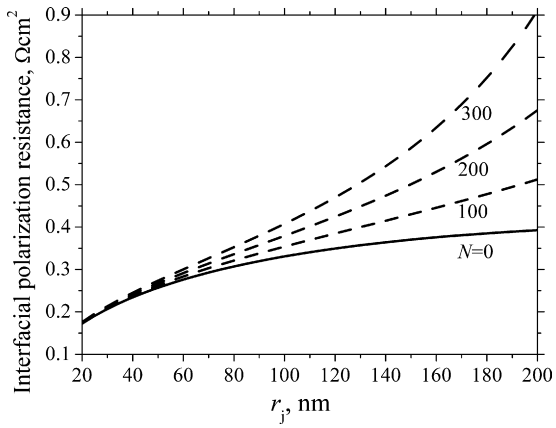

Fig. 3. The effects of impregnated particle size on interfacial polarization resistance for LSC–SDC nanostructured electrode ($\phi_i = \phi_j = 0.5$, $\phi_g = 0.41$, $r_i = 0.5$ μm, and RT–800 °C cycle).

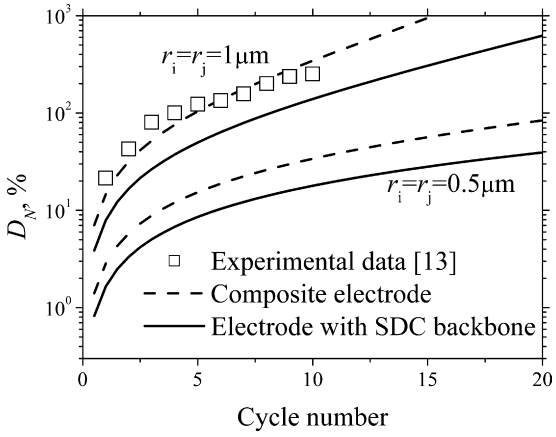

Fig. 4. Degradation rate, D_N, of LSC–SDC electrode with SDC backbone structure (the same structure as the nanostructured electrode) and composite LSC–SDC electrode as a function of RT–800 °C cycle number.

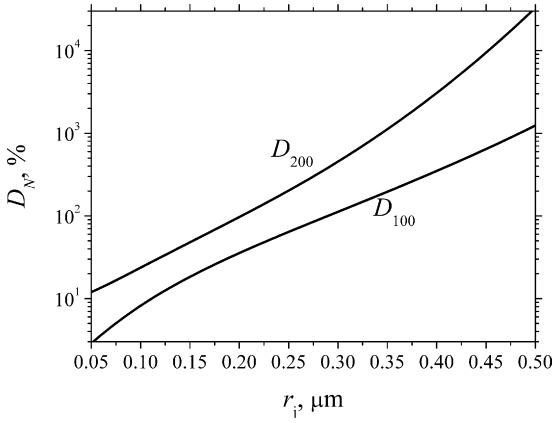

Fig. 5. Degradation rate, D_N, of nanostructured LSC–SDC electrode as a function of impregnated particle size ($\phi_i = \phi_j = 0.5$, $\phi_g = 0.41$, $r_i = 1$ μm, and RT–800 °C cycle).

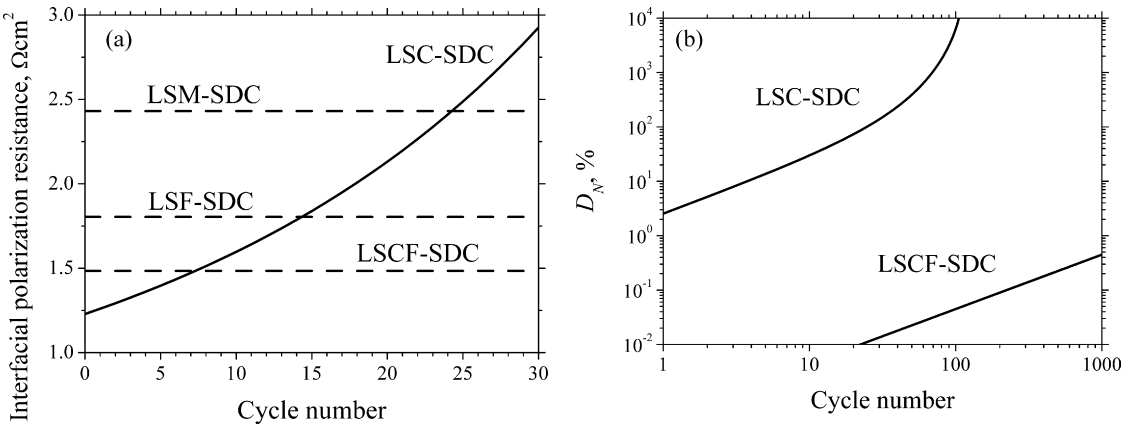

Fig. 6. Durability of typical composition cathodes. (a) Interfacial polarization resistance for LSC–SDC, LSM–SDC, LSF–SDC and LSCF–SDC composite cathodes ($\phi_i = \phi_j = 0.5$, $\phi_g = 0.41$, $r_i = r_j = 0.5$ μm, and RT–800 °C cycle). (b) Degradation rate, D_N, of LSC and LSCF based cathodes. The degradation rates of LSF and LSM are not shown since they are much smaller than that of LSCF.

3.4. Effects of TEC mismatch

The model quantitatively predicts the durability of composite cathodes composed of typical electrocatalysts. TECs of the electrocatalysts are usually higher than those of electrolytes. Therefore, performance degradation cannot be kept away from thermal cycle processes. So, the relationship between degradation rate and TEC is of great interest for SOFC development. However, such a relation is not quantitatively clear till now although less degradation is generally expected for lower TEC difference. Our model can predict the degradation rate of a composite cathode based on the electrocatalyst's TEC. Fig. 6a shows the interfacial polarization resistances of typical composite cathodes that undergo RT–800 °C thermal cycle. For a fresh sample, LSC (TEC = 23×10^{-6} K^{-1}) based cathode has the lowest resistance due to the highest catalytic activity. However, after 7 cycles, its resistance is comparable to that of LSCF ($La_{0.6}Sr_{0.4}Co_{0.2}Fe_{0.8}O_{3+\delta}$, TEC = 14.8×10^{-6} K^{-1}). After 14 cycles, the performance is almost the same as LSF ($La_{0.8}Sr_{0.2}FeO_{3+\delta}$, TEC = 12.3×10^{-6} K^{-1}). And after 25 cycles, the cathode exhibits worse performance than LSM ($La_{0.8}Sr_{0.2}MnO_{3+\delta}$, TEC = 11.7×10^{-6} K^{-1}). On the contrary, fresh LSM sample has the highest stability and the lowest electrode performance as expected. However, Fig. 6b suggests that LSCF is pretty stable although its TEC is 35% higher than the electrolyte's (TEC = 11×10^{-6} K^{-1}), $D_{100} \approx 0.04\%$ and $D_{1000} \approx 0.4\%$. Considering its much lower R_0 than LSM's or LSF's, LSCF should be a competitive electrocatalyst for intermediate-temperature SOFCs that operated below 800 °C.

The model provides a remarkable ability to balance thermal-expansion restriction and catalytic requirement of cathode materials. Electro-catalytic activity and TEC of typical perovskite electrocatalysts, $La_{1-x}Sr_x(Mn–Fe–Co)O_{3-\delta}$, are determined mainly by their composition. Usually, a highly active electrocatalyst also has large TEC. Further, both the electrocatalytic activity and TEC increase with the increase of Co content in the $La_{1-x}Sr_x(Mn–Fe–Co)O_{3-\delta}$ system [16]. Therefore, a highly active electrocatalyst often results in low durability in thermal cycle processes. Considering the cost and practical application, a degradation limit should be set for all SOFC components. Our model can predict the acceptable TEC mismatch for a given practical limit, thus provides an insight into material development. For example, if the limit is $D_{100} < 0.1\%$, the predicted TEC should be less than 15.1×10^{-6} K^{-1}. In this case, LSCF, LSF and LSM meet the restriction (Fig. 7). But LSCF is the best since LSCF has the highest electrochemical activity among them. If the limit is not so tough, $D_{100} < 1\%$, an electrocatalyst with TEC of 16.6×10^{-6} K^{-1} is good enough. In this case, LSCF is still a good choice. A better choice should be made with Co content higher than that in LSCF, 0.2, and, if the chemical compatibility is not of concern, it should be increased to a level as long as the TEC reaches the upper limit so that the electrochemical activity can be as high as possible. It is noted that TECs of LSC, $Ba_{0.5}Sr_{0.5}Co_{0.8}Fe_{0.2}O_{3-\delta}$, and $Sm_{0.5}Sr_{0.5}CoO_{3-\delta}$ are so high that they do not gratify a limit of $D_{10} < 1\%$.

3.5. Effects of electrode composition

The model can optimize electrode composition so that the composite cathode can achieve high durability and electrochemical activity. Composite cathodes, which are formed by adding the electrolytes to the electrocatalysts, are practically used to minimize the TEC mismatch in addition to increasing TPB length [7]. Theoretically, TEC of the whole composite electrode decreases with the increase of electrolyte content [9] (Fig. 8, curve α_{ave}). This infers that high electrolyte content results in low composite TEC, and might further suggest high durability in thermal cycle processes. Our model demonstrates that the relation between the content and the durability is much more complicated. In the low range, the durability increases rapidly when the content exceeds the electrolyte percolation limit (Fig. 8, curve D_N). In the high range, the durability decreases remarkably when the content approaches the electrocatalyst percolation limit. In the middle range, the durability waves

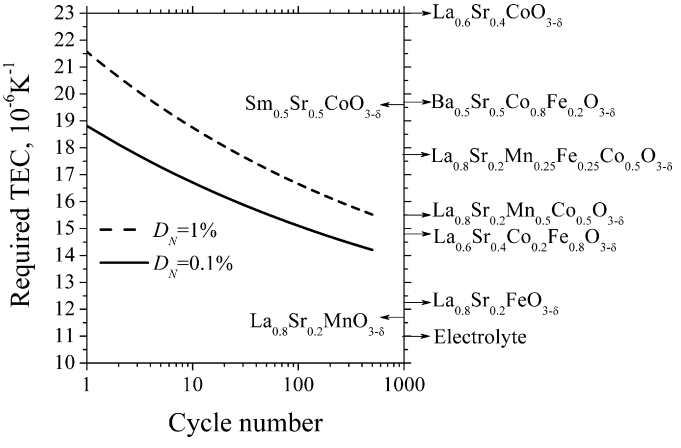

Fig. 7. Required electrocatalyst TEC for degradation rates of 0.1 and 1% of SDC-based composite cathodes in RT–800 °C cycle processes. TEC data in Refs. [13,15,16] of typical electrocatalysts is also indicated in the figure ($\phi_i = \phi_j = 0.5$, $\phi_g = 0.41$, $r_i = r_j = 0.5$ μm, and RT–800 °C cycle).

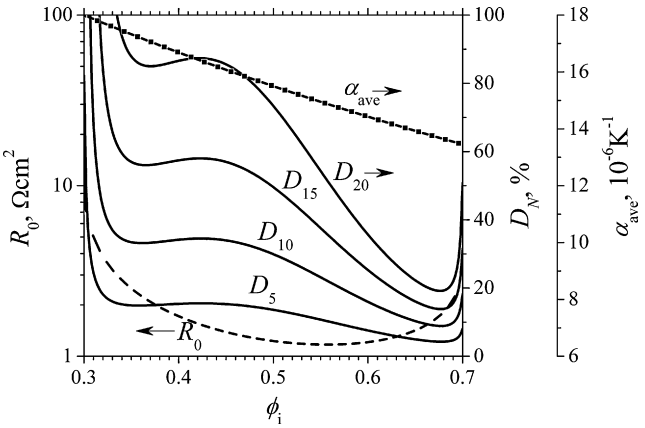

Fig. 8. The effects of cathode composition on interfacial polarization resistance for fresh LSC–SDC composite cathode, R_0; TEC of composite cathode, α_{ave}; and degradation rate, D_N, for RT–800 °C cycle (ϕ_g = 0.41 and $r_i = r_j$ = 0.5 μm).

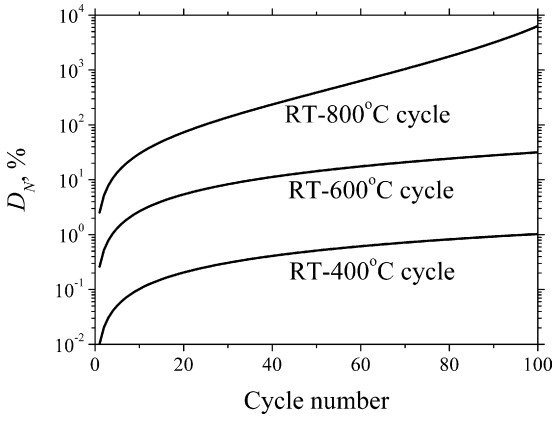

Fig. 10. Degradation rate, D_N, of LSC–SDC composite electrode as a function of cycle number ($\phi_i = \phi_j$ = 0.5, ϕ_g = 0.41, and $r_i = r_j$ = 0.5 μm).

with the content once, but the change is not significant. At the composition where the highest performance is achieved for the fresh sample (Fig. 8, curve R_0), the stability is not the highest, but also not too bad. This composition might be safe since Fig. 8 suggests the percolated range shrinks when the cycle number increases. This is also explicitly shown in Fig. 9, and it suggests that the lower/upper threshold of SDC volume fraction increases/decreases with the increase of thermal cycle times. This trend is significant when a big LSC particle is used. For example, in case r_j = 1 μm, no reasonable performance can be theoretically maintained after 50 RT–800 °C thermal cycles. It also suggests that the lifetime of composite electrode upon thermal cycle can be extended by utilizing small LSC particle size combining with a proper SDC volume fraction. Therefore, the practical composition should be also determined by the proposed cycle number rather than starting from the electrolyte percolation limit as suggested in the literature [30].

3.6. Effects of temperature difference

The model exhibits that high durability can be obtained when the temperature change (ΔT) is small (Fig. 10). For example, D_{100} is only 31.7% for RT–600 °C cycle while it is 6358% for RT–800 °C cycle. This suggests increased reliability while reducing operating temperature, adding advantages to reduced temperature SOFCs, especially the low-temperature SOFCs that operated below 600 °C. The model also infers that TEC mismatch is not so critical for electrochemical devices that operated at relatively low temperatures such as sodium sulfur batteries. The model also exhibits that, for composite electrodes, small particle size results in high durability (Fig. 11). Such relation infers low-temperature processing techniques including sol–gel [31], and combustion chemical vapor deposition [32] is more promise in fabricating composite cathodes than high-temperature related processes such as screen-printing and co-firing, which result in large particles.

3.7. Durability of Ni-YSZ anodes

The model is also applicable to cermet anodes consisting of oxygen-ion conducting ceramics and electronic conducting metal such as nickel. Fig. 12a shows the durability comparison between the model prediction and literature data for a Ni-YSZ anode that has undergone 100–1000 °C thermal cycles [33]. Only slight degradation is predicted due to the TEC mismatch between Ni and YSZ. The prediction is consistent very well with the experimental description that the interfacial polarization resistance is stable within the experimental uncertainty [33]. For example, after 8 cycles, the interfacial polarization resistance is 0.18 Ω cm^2, which is very close to 0.19 Ω cm^2, the experimental result. Fig. 12b shows the anode durability as a function of thermal cycle number. D_{100} for Ni-YSZ anodes consisting of submicro particles ($r_i = r_j$ = 0.5 μm) is about 4.3%. Although the durability is worse than that of LSCF-based composite electrode ($D_{100} \approx$ 0.04%, Fig. 6b), it is good enough for present SOFC demonstration. It should be noted that, due to the volume threshold increases with the cycle number, the Ni volume percent

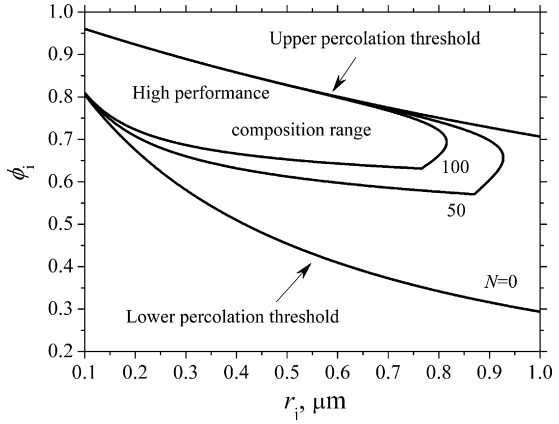

Fig. 9. The evolution of SDC volume fraction thresholds as a function of thermal cycle number and LSC particle size for the LSC–SDC composite cathode ($\phi_{io} = \phi_{el}$ = 0.5, ϕ_g = 0.41, r_i = 1 μm, and RT–800 °C cycle).

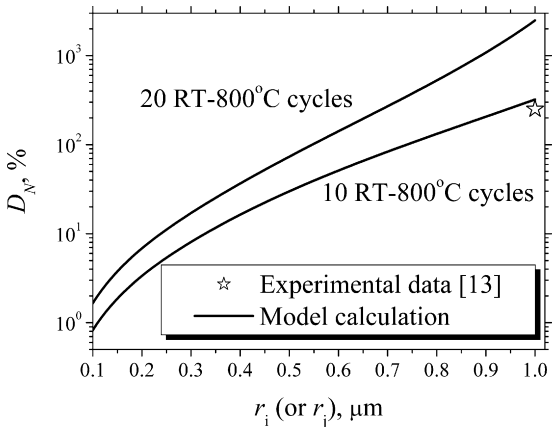

Fig. 11. Degradation rate, D_N, of LSC–SDC composite electrode as a function of particle size ($\phi_i = \phi_j$ = 0.5, ϕ_g = 0.41, and $r_i = r_j$).

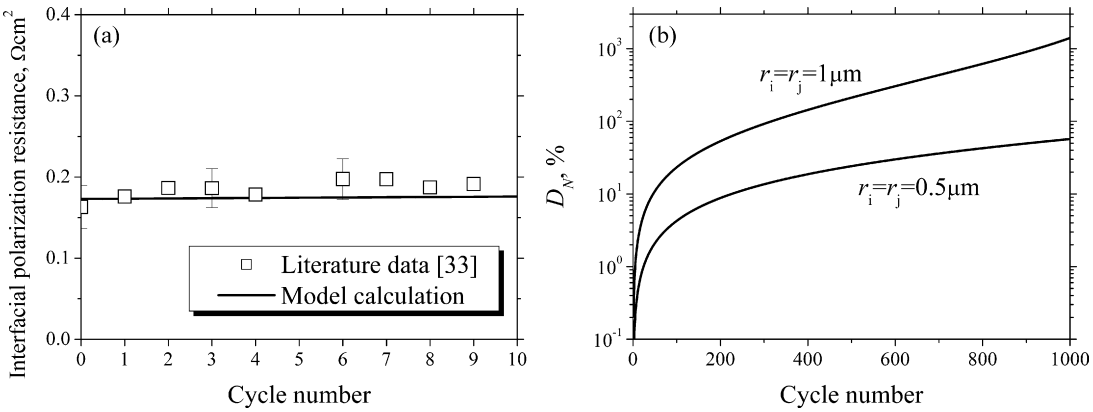

Fig. 12. Interfacial polarization resistances at 1000 °C for a Ni-YSZ anode as a function of 100–1000 °C cycle number. (a) Model validation. (b) Long-term prediction (ϕ_i = 0.6, ϕ_j = 0.4, ϕ_g = 0.41, and r_i = r_j = 1 μm) [33].

should be high than 30%, the typical percolation limit for Ni in a porous cermet anode. This might be one of the reasons that the practical Ni/YSZ volume ratio is usually 40/60.

3.8. Single cell durability in thermal cycle processes

The model is further validated with experimental data for a microtubular single cell consisting of a Ni-YSZ anode, an YSZ electrolyte, and a LSM–YSZ cathode. The durability of a single cell in thermal cycle processes depends not only on the stability of its anode and cathode but also on the stability of the electrolyte and sealing material. The sealing effect can be effectively minimized using the tubular structure. And the electrolyte degradation is negligible [35]. Thus, the performance degradation is dominated by the electrode stability. The power export, W_N, after N cycles under constant current density can be estimated as:

$$W_N = IV_{ocv} - I^2[R_0^E + R_0^C(1 + D_N^C) + R_0^A(1 + D_N^A)] \quad (9)$$

where V_{OCV} denotes open-circuit voltage, I the current density. R_0^E, R_0^C and R_0^A represent the area-specific resistances of electrolyte, cathode and anode for a fresh single cell, respectively. D_N^C and D_N^A are the durability of the cathode and anode, respectively. Fig. 13 shows the comparison between prediction and experiment. The parameters are set based on the report by Campana et al. [34] and listed in Table 1. The model calculation basically agrees with literature data. It is predicted that the power density decreases by 0.4% after 100 thermal cycles. It is noted that the single cell durability is determined mainly be the anode since the degradation of LSM–YSZ cathode is not so significant than that of Ni-YSZ anode due to the smaller TEC mismatch between LSM and YSZ.

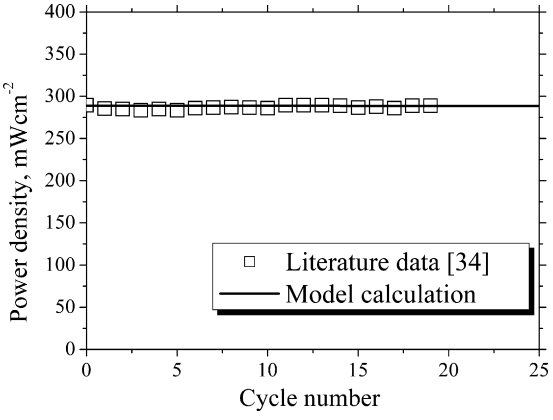

Fig. 13. Power density of a single Ni-YSZ/YSZ/LSM–YSZ cell as a function of RT–900 °C cycle number (ϕ_i = ϕ_j = ϕ_g = 0.5 and r_i = r_j = 1 μm) [34].

4. Conclusions

The durability model relates the degradation rate to particle interface evolution in thermal cycle processes and is briefly summarized as follows: temperature change induces thermal stresses, which break the interfaces, reduces three-phase boundaries and conductivities, and consequently degrades electrode performance. The degradation rate is formulated as a function of thermal expansion coefficient, temperature change, cycle number, and electrode structure features including particle size, composition, and porosity. The model prediction is consistent with previous experimental results. The model demonstrates that small particle size results in not only high electrochemical activity but also excellent durability. The model reveals that nanostructured electrodes have excellent electrochemical activity and remarkable durability, suggesting that these electrodes can substantially enhance the overall SOFC performance. The model points out that the percolated zone of a composite cathode shrinks with the cycle number, suggesting the composition should be optimized with respect to electrode activity and durability. The model can predict the required TEC for a given durability, giving a clear clue for material development. Finally, the model provides remarkable ability in predicting the thermal-cycle durability of solid-state electrochemical devices when the mechanical, electrochemical and structural parameters are available.

Acknowledgements

This work is supported by the Natural Science Foundation of China (10979046 and 50730002) and the Ministry of Science and Technology of China (2007AA05Z151).

References

[1] Z.P. Shao, S.M. Haile, Nature 431 (2004) 170–173.
[2] A. Atkinson, S. Barnett, R.J. Gorte, J.T.S. Irvine, A.J. McEvoy, M. Mogensen, S.C. Singhal, J. Vohs, Nat. Mater. 3 (2004) 17–27.
[3] S.W. Tao, J.T.S. Irvine, Nat. Mater. 2 (2003) 320–323.
[4] L. Yang, S.Z. Wang, K. Blinn, M.F. Liu, Z. Liu, Z. Cheng, M.L. Liu, Science 326 (2009) 126–129.
[5] T. Suzuki, Z. Hasan, Y. Funahashi, T. Yamaguchi, Y. Fujishiro, M. Awano, Science 325 (2009) 852–855.
[6] A. Nakajo, C. Stiller, G. Harkegard, O. Bolland, J. Power Sources 158 (2006) 287–294.
[7] S.B. Adler, Chem. Rev. 104 (2004) 4791–4843.
[8] R.W. Rice, J. Mater. Sci. 40 (2005) 983–989.
[9] C.S. Montross, H. Yokokawa, M. Dokiya, Br. Ceram. Trans. 101 (2002) 85–93.
[10] Z.P. Bazant, Probab. Eng. Mech. 19 (2004) 307–319.

[11] Y. Paramonov, J. Andersons, Compos. Part A: Appl. Sci. Manuf. 38 (2007) 1227–1233.
[12] Y. Zhang, C. Xia, J. Power Sources 195 (2010) 4206–4212.
[13] F. Zhao, R.R. Peng, C.R. Xia, Mater. Res. Bull. 43 (2008) 370–376.
[14] M.T. Todinov, Int. J. Solids Struct. 46 (2009) 887–901.
[15] A. Nakajo, Z. Wuillemin, J. Van herle, D. Favrat, J. Power Sources 193 (2009) 203–215.
[16] F. Tietz, I.A. Raj, M. Zahid, D. Stover, Solid State Ionics 177 (2006) 1753–1756.
[17] Y.S. Chou, J.W. Stevenson, T.R. Armstrong, L.R. Pederson, J. Am. Ceram. Soc. 83 (2000) 1457–1464.
[18] K. Sato, H. Yugami, T. Hashida, J. Mater. Sci. 39 (2004) 5765–5770.
[19] N. Orlovskaya, M. Lugovy, S. Pathak, D. Steinmetz, J. Lloyd, L. Fegely, M. Radovic, E.A. Payzant, E. Lara-Curzio, L.F. Allard, J. Kuebler, J. Power Sources 182 (2008) 230–239.
[20] A. Julian, E. Juste, P.M. Geffroy, N. Tessier-Doyen, P. Del Gallo, N. Richet, T. Chartier, J. Eur. Ceram. Soc. 29 (2009) 2603–2610.
[21] A. Selcuk, A. Atkinson, J. Eur. Ceram. Soc. 17 (1997) 1523–1532.
[22] F.S. Baumann, J. Fleig, G. Cristiani, B. Stuhlhofer, H.U. Habermeier, J. Maier, J. Electrochem. Soc. 154 (2007) B931–B941.
[23] X.J. Chen, S.H. Chan, K.A. Khor, Electrochim. Acta 49 (2004) 1851–1861.
[24] D. Son, J.J. Kim, J.Y. Kim, D. Kwon, Mater. Sci. Eng. A 406 (2005) 274–278.
[25] W. Zhu, D. Ding, C.R. Xia, Electrochem. Solid-State Lett. 11 (2008) B83–B86.
[26] S.P. Jiang, Mater. Sci. Eng. A 418 (2006) 199–210.
[27] J.M. Vohs, R.J. Gorte, Adv. Mater. 21 (2009) 943–956.
[28] T.Z. Sholklapper, H. Kurokawa, C.P. Jacobson, S.J. Visco, L.C. De Jonghe, Nano Lett. 7 (2007) 2136–2141.
[29] T.Z. Sholklapper, C.P. Jacobson, S.J. Visco, L.C. De Jonghe, Fuel Cells 8 (2008) 303–312.
[30] V. Dusastre, J.A. Kilner, Solid State Ionics 126 (1999) 163–174.
[31] C.R. Xia, Y.L. Zhang, M.L. Liu, Electrochem. Solid-State Lett. 6 (2003) A290–A292.
[32] Y. Liu, S.W. Zha, M.L. Liu, Adv. Mater. 16 (2004) 256–260.
[33] S. Primdahl, M. Mogensen, J. Appl. Electrochem. 30 (2000) 247–257.
[34] R. Campana, R.I. Merino, A. Larrea, I. Villarreal, V.M. Orera, J. Power Sources 192 (2009) 120–125.
[35] J.H. Joo, G.M. Choi, Electrochem. Solid-State Lett. 13 (2010) B17–B20.